Article

Modeling the Mechanosensitivity of Neutrophils Passing through a Narrow Channel

Tenghu Wu[1] and James J. Feng[2,*]

[1]Department of Chemical and Biological Engineering and [2]Department of Chemical and Biological Engineering and Department of Mathematics, University of British Columbia, Vancouver, British Columbia, Canada

ABSTRACT   Recent experiments have found that neutrophils may be activated after passing through microfluidic channels and filters. Mechanical deformation causes disassembly of the cytoskeleton and a sudden drop of the elastic modulus of the neutrophil. This fluidization is followed by either activation of the neutrophil with protrusion of pseudopods or a uniform recovery of the cytoskeleton network with no pseudopod. The former occurs if the neutrophil traverses the narrow channel at a slower rate. We propose a chemo-mechanical model for the fluidization and activation processes. Fluidization is treated as mechanical destruction of the cytoskeleton by sufficiently rapid bending. Loss of the cytoskeleton removes a pathway by which cortical tension inhibits the Rac protein. As a result, Rac rises and polarizes through a wave-pinning mechanism if the chemical reaction rate is fast enough. This leads to recovery and reinforcement of the cytoskeleton at the front of the neutrophil, and hence protrusion and activation. Otherwise the Rac signal returns to a uniform pre-deformation state and no activation occurs. Thus, mechanically induced neutrophil activation is understood as the competition between two timescales: that of chemical reaction and that of mechanical deformation. The model captures the main features of the experimental observation.

INTRODUCTION

Neutrophils are a key part of the immune system. In its inactive state in vascular flow, the neutrophil has a spherical shape with a diameter of ~10 μm (1,2). Upon activation, the neutrophil deforms and extends pseudopods. Under the guidance of cytokines, it migrates through endothelial slits toward the inflammation site (3). In this process, the activated cell undergoes large mechanical deformation and morphological changes. Thus the biophysical properties of the neutrophil are crucial to its function.

Aside from chemical signals, neutrophils are also sensitive to mechanical forcing and deformation (4–9). For example, a gentle fluid flow over a crawling neutrophil causes it to stop crawling and return to a spherical shape (5–7). Apparently, a mild shear stress inhibits neutrophil activation. Stronger forcing in micropipette aspiration, on the other hand, triggers actin polymerization inside the aspirated tongue and formation of protrusions (4). This points to stress-induced activation of the neutrophil. Later, Yap and Kamm (8,9) passed neutrophils through microfluidic channels and filters, and found that the mechanical deformation may activate the neutrophils with formation of pseudopods.

These seemingly contradictory responses of neutrophil to mechanical deformation can be rationalized by the FLNa-FilGAP pathway (10,11). Filamin A (FLNa) crosslinks actin filaments and recruits the FilGAP protein, a known Rac inhibitor, from the cytosol. When deformed by external forc-

ing, FLNa releases FilGAP to the membrane where it inhibits Rac (10,11). When neutrophil is under mild forcing, such a FLNa-FilGAP pathway leads to Rac inhibition and neutrophil deactivation (5–7). In micropipette aspiration, on the other hand, the severe cell deformation causes the actomyosin network to detach from the plasma membrane (4) and voids the FLNa-FilGAP pathway. Thus, Rac remains highly active on the membrane to induce cortex growth and new protrusion. This explains the observation that neutrophil is deactivated by mild shear stress but activated by severe deformation. Note that the FLNa-FilGAP pathway relies on the cortical tension, and is distinct from the global inhibition of protrusion by the plasma membrane tension (12).

However, the experiments of Yap and Kamm (8,9) raise further questions on how the neutrophil responds to mechanical forces. In forcing neutrophils through microfluidic channels, Yap and Kamm (8) found that the neutrophil fluidizes upon entering the narrow channel, with its cortex disassembling and its elastic modulus dropping sharply. This allows the neutrophil to flow into the channel as if it were a liquid drop. Fluidization likely has a mechanical origin, with mechanical deformation breaking the actin crosslinks or rupturing the actin filaments (8,9), ultimately leading to the disintegration of the cell cortex. Once inside the microfluidic channel, the neutrophil becomes activated and develops pseudopodia to explore its surroundings. The time required for neutrophil activation is sensitive to temperature, suggesting that activation is regulated by chemical signals such as the Rho GTPases. Yap and Kamm (9) further probed the activation criterion by filtering neutrophils at different

CrossMark

rates. Under a fast rate, the F-actin content drops suddenly and then grows back uniformly in the cell without formation of pseudopods. Under a slow rate, the cell does activate and form pseudopods. Yap and Kamm (9) reasoned that the entry time t_e, defined as the time between the front of the cell reaching the opening of the narrow channel and its rear clearing the opening, must be sufficiently long to give the cell enough time to be activated. Pseudopods form under protrusion forces due to actin polymerization, which is modulated by the Rho GTPases including Rac (13). In the experiment (9), $t_e \approx 15$ s for the slow filtration rate and 2 s for the fast filtration rate. These are comparable to the reciprocal of the kinetic rate of the Rho GTPases (14–16). These findings offer further evidence for a Rho-GTPases-based pathway for neutrophil activation after fluidization.

This work is motivated by the experiments of Yap and Kamm (8,9), and aims to investigate these outstanding questions: 1) How do the Rho GTPases and FLNa-FilGAP pathways govern the activation process? 2) How is activation affected by the competing timescales of cell entry and chemical reaction? 3) How does the cell cortex recover with or without activation? Our objective is to synthesize hypotheses and ideas from prior experiments and modeling into a quantitative framework for describing and predicting the fluidization and activation of neutrophils. This will be realized in a biomechanical model that couples chemical signaling with cell movement and membrane deformation in a fluid environment.

MATERIALS AND METHODS

Neutrophil model

Our two-dimensional (2D) study of neutrophil transit through a narrow channel strives to capture not only the overall mechanics of cell deformation and fluid flow, but also the intracellular remodeling that characterizes fluidization and activation. Therefore, our neutrophil model accounts for mechanics of the cell membrane, kinetics of chemical signaling, and cytoskeletal remodeling. In the following subsections, we will discuss each of the three components. As the nucleus and other cytoplasmic organelles play no role in the phenomenon of interest, they will not be explicitly modeled.

Membrane mechanics

What we call "the membrane" in the model represents two biological entities: the plasma membrane and the underlying cytoskeleton or cortex. In this study, the two never detach from each other. Thus it is convenient to represent both using a single mechanical element, a 2D loop discretized into elastic segments. Nevertheless, the biological picture of the two separate components informs the modeling of the mechanics of the membrane. For example, although the plasma membrane can sustain very limited strain (5%) before rupture (17), wrinkles provide excess surface area and allow large elastic deformation. The cortex, a thin polymer network of crosslinked F-actin and myosin motors, is prestressed in the rest state due to myosin contraction. These features will be accounted for in the membrane model.

In our 2D model, we represent the membrane by N elastic segments connected at N nodes into a loop. The ith node is at $\mathbf{X}_i$, and the ith edge has length $l_i = |\mathbf{X}_i - \mathbf{X}_{i-1}|$. In the initial, undeformed shape, the loop is a circle of diameter d, and all the edges have the same resting length $l_0 = d\sin(\pi/N)$. On the ith edge, the plasma membrane produces a linearly elastic tension,

$$\sigma_m^i = E_m\left(\frac{l_i - l_0}{l_0}\right), \tag{1}$$

where E_m is Young's modulus of the plasma membrane. The cortex also contributes a tension on the ith edge,

$$\sigma_\tau^i = E_c^i \varepsilon_i, \tag{2}$$

where E_c^i is the cortical modulus, and ε_i is the prestrain of the cortex due to myosin motors (18,19). E_c^i is not a constant but will vary along the cell membrane and in time during cell fluidization and activation. It will be used to indicate the integrity of the actomyosin cortex. As myosin phosphorylation is regulated by the Rho family of GTPases (20), we will relate the prestrain ε_i to the local level of GTPases in our kinetic model (see Eq. 14). For out-of-plane bending of both the plasma membrane and the cortex, we adopt the bending energy (21–23)

$$E_b = \frac{k_b}{2}\sum_{j=1,N}\tan^2\left(\frac{\Theta_j}{2}\right), \tag{3}$$

where k_b is the bending modulus, and Θ_j is the angle between the jth and $(j+1)$th edges. Thus, we assume zero spontaneous curvature in the membrane.

We also impose an energy penalty against changes in cell volume (or cell area in our 2D model):

$$E_v = k_v\left(\frac{A - A_0}{A_0}\right)^2. \tag{4}$$

This constraint is motivated more by numerical than physical considerations. In principle, incompressibility for the fluid inside and outside the cell should ensure cell-area conservation. Because of numerical errors, however, area variation can become a concern when the cell undergoes severe deformation. Hence, this seemingly superfluous constraint has been widely used in red blood cell models (23–25). In our model, it limits area variations to 1%.

To simulate a cell passing through a narrow channel, a repulsive force is commonly introduced between the cell membrane and the channel wall to avoid overlap. Our simulation uses the virtual spring model (26–28) to activate a repulsive force when the membrane-wall clearance falls below twice the grid size. The stiff virtual springs keep the clearance from narrowing further without interfering with the cell dynamics otherwise (28).

Lastly, we include a protrusion force on the cell membrane due to the growing cytoskeleton underneath. This is intended to capture the formation of pseudopods during activation. In vivo experimental data show that protrusion follows activation of Rac at the leading edge (29). Following previous models (30), we express the protrusion force on the ith node as a function of the active Rac on the membrane,

$$\mathbf{F}_{pro}^i = k_{pro}\overline{a}_i\mathbf{n}_i - \frac{k_{pro}}{N}\sum_{j=1,N}\overline{a}_j\mathbf{n}_j, \tag{5}$$

where k_{pro} is a protrusion coefficient, and $\overline{a}_i = (1/2)(a_i l_i + a_{i+1}l_{i+1})/(l_0 a_0)$ is the average of the active Rac on the two neighboring edges scaled by the initial Rac on each edge, with a_i being the Rac concentration on the ith edge and a_0 being the initial concentration. The $\mathbf{n}_i$ is the unit outward normal on the ith node, which bisects the angle between the adjacent edges. The first term is the protrusion force intended for the forefront of the cell, where Rac is expected to build up (more details in the next section). The second term represents the reaction force. As the neutrophil will not be anchored onto a substrate via focal adhesion, the protrusion force must be balanced by backward forces on the membrane in the rear. Thus, the sum of $\mathbf{F}_{pro}^i$ over the cell periphery vanishes.

Collecting all the forces discussed above, we write the total force acting on the ith membrane node as

$$\mathbf{F}^i = \mathbf{F}_m^i + \mathbf{F}_\tau^i + \mathbf{F}_{\text{pro}}^i + \frac{\partial(E_b + E_v)}{\partial \mathbf{X}_i}, \qquad (6)$$

where $\mathbf{F}_m^i = (\sigma_m^{i+1}\boldsymbol{\tau}_{i+1} - \sigma_m^i\boldsymbol{\tau}_i)$ and $\mathbf{F}_\tau^i = (\sigma_\tau^{i+1}\boldsymbol{\tau}_{i+1} - \sigma_\tau^i\boldsymbol{\tau}_i)$ are the tensions on node i due to the plasma membrane and cortex, respectively. The value $\boldsymbol{\tau}_i$ is the unit vector along the ith edge, pointing from the $(i-1)$th to the ith node.

Kinetics of chemical signaling

Typically, the polarity of the neutrophil is characterized by anisotropic distribution of the Rho family of GTPases, such as Rac, RhoA, and Cdc42. Prior experimental data and modeling show an antagonism between Rac and RhoA that is modulated by Cdc42, and that Rac serves as an indicator of cell polarization (31,32). Thus, we will use Rac as the sole marker for neutrophil polarity in our model, and will not account for RhoA and Cdc42 separately.

In the model, Rac has an active, membrane-bound state and an inactive state in the cytoplasm. The active Rac is defined as a concentration a_i on the ith edge of the membrane, while the inactive cytosolic Rac is given by I. The two are related by the conservation of the total amount of Rac:

$$I + \sum_{i=1}^{N} a_i l_i = 1. \qquad (7)$$

Thus, we have scaled both a_i and I by the total amount of Rac, such that I is dimensionless, and a_i has the dimension of the reciprocal of length.

The active Rac evolves according to a discretized reaction-diffusion equation,

$$\frac{d(a_i l_i)}{dt} = k_+ \frac{l_i}{d} I - k_-(a_i l_i) + (q_i - q_{i-1}). \qquad (8)$$

On the right-hand side, the first term represents Rac attachment and activation, $(l_i/d)I$ being the inactive Rac available to the edge. The on-rate is written as

$$k_+ = k_{\text{on}} + \frac{\gamma a_i^2}{K^2 + a_i^2}, \qquad (9)$$

where the Hill function is introduced to stabilize a polarized state by wave-pinning (33–35). The second term represents downregulation of the membrane-bound active Rac, with

$$k_- = k_{\text{off}} + k_\tau \sigma_\tau^i \qquad (10)$$

incorporating the inhibition of Rac by cortical tension σ_τ through the FLNa-FilGAP pathway (10,11). The last term on the right-hand side of Eq. 8 represents 1D diffusion of active Rac along the membrane, with

$$q_i = D \frac{a_{i+1} - a_i}{\frac{1}{2}(l_i + l_{i+1})} \qquad (11)$$

being the diffusive flux from edge l_{i+1} to edge l_i at node i, with D being the diffusivity. As the signaling proteins diffuse ~100 times faster in the cytosol than on the membrane (16), we assume that the inactive I is uniformly available to membrane attachment and activation. Now Eq. 8 can be written as an evolution equation for $a_i(t)$,

$$\dot{a}_i = \left(k_{\text{on}} + \frac{\gamma a_i^2}{K^2 + a_i^2}\right)\frac{I}{d} - \left(k_{\text{off}} + k_\tau \sigma_\tau^i\right)a_i - \frac{a_i \dot{l}_i}{l_i} + D\nabla_i^2 a_i, \qquad (12)$$

where the dot indicates the time derivative, and ∇_i^2 is the discretized form of the Laplacian:

$$\nabla_i^2 a_i = 2\frac{a_{i+1}(l_i + l_{i-1}) - a_i(l_{i-1} + 2l_i + l_{i+1}) + a_{i-1}(l_i + l_{i+1})}{(l_i + l_{i+1})l_i(l_i + l_{i-1})}. \qquad (13)$$

Once the neutrophil is polarized, it is known that Rac is enriched in the front and promotes F-actin growth, while RhoA is concentrated in the rear and promotes myosin contraction (29,36). Because our model does not explicitly account for RhoA or myosin, we represent the polarity in myosin contraction indirectly via the prestrain ε_i (Eq. 2):

$$\varepsilon_i = \varepsilon(a_i) = \varepsilon_0 \exp\left[k\left(1 - \frac{a_i}{a_i^0}\right)\right]. \qquad (14)$$

Thus, the prestrain ε, and the cortical tension σ_τ by extension, are inhibited by the high Rac in the front, and promoted by the low Rac (and implicitly high RhoA) at the rear. The coefficient k and the prestrain of the resting state ε_0 are taken to be constants. The exponential form is used for its simplicity; it recovers the equilibrium state $\varepsilon = \varepsilon_0$ when $a = a_0$, and naturally represents the decline of the cortical tension with increasing a.

Remodeling of the cytoskeleton

As mentioned above, our model does not represent the cytoskeleton by a physical element separate from the plasma membrane, but uses the cortical modulus E_c to indicate the density and integrity of the cortex. The dynamics of E_c is regulated by mechanical perturbations as well as chemical signals. It can be reduced to zero by severe deformation (37–40), and then grow back under the promotion of Rac. Considering experimental evidence that the actomyosin network disassembles much more easily under bending than stretching (37–39), we assume that the cortex disassembles catastrophically when the instantaneous bending rate exceeds a threshold,

$$\text{If } \frac{\dot{\theta}_i}{\Theta_0} > \beta, \qquad (15)$$
$$\text{then } E_c^i = 0,$$

where β is a critical bending rate constant; $\Theta_0 = 2\pi/N$ is the initial angle between adjacent segments; and $\dot{\theta}_i = (1/2)|\dot{\Theta}_{i-1} + \dot{\Theta}_i|$ is the bending rate of the ith edge, calculated by averaging the bending rates at the two end nodes. The underlying physical assumption is that if the cortex is bent at a rate that exceeds the maximum that the cytoskeleton can accommodate by remodeling, the network will rupture and disintegrate.

Active Rac promotes actin polymerization and strengthens the local actomyosin network (41). Consistent with this, Yap and Kamm (9) documented high concentration of F-actin localized at the protrusion front. Based on these, we model cortical recovery after fluidization by

$$\dot{E}_c^i = k_{\text{poly}}\frac{a_i}{a_0}\left(E_c^0 - E_{\text{avg}}\right), \qquad (16)$$

where k_{poly} is a polymerization rate for the cytoskeletal network, and E_{avg} is the average modulus over the entire membrane at this time. Note that we use the instantaneous average modulus E_{avg}, instead of the local E_c^i, to moderate the cytoskeletal reconstitution. This is motivated by the fact that cytoskeletal growth is fueled by actin polymerization, and in our model E_{avg} indicates the amount of F-actin in the cortex. Once E_{avg} recovers to E_c^0, the cortex has reached the same strength, in an average sense, as in the resting state. Then the balance between G-actin and F-actin has returned to homeostasis, and the cytoskeleton ceases to grow further. Besides, this formulation allows E_c to grow beyond E_c^0 at protruding pseudopods in the activated neutrophil (see Activation, below).

Computational setup and model parameters

The computational domain is a rectangular channel with a constriction (Fig. 1). Periodic boundary conditions are imposed between the entrance and the exit, whereas no-slip conditions prevail on the solid walls. A pressure drop ΔP is imposed across the length of the domain L_x, which sustains the channel flow. In the experiment of Yap and Kamm (9), the neutrophil is collected in a quiescent reservoir after filtration. In the simulation, therefore, we set the pressure drop ΔP to zero once the cell's centroid reaches 1.8d outside the exit of the constriction. Afterwards it may relax in an essentially quiescent medium as in the experiment.

The numerical computation consists mostly in solving for the fluid flow inside and outside the neutrophil and the deformation of the cell membrane. This fluid-structure interaction problem is handled using the immersed boundary method (42,43). The dynamics of Rac and cortical modulus E_c takes place on the cell membrane; these one-dimensional problems add little to the computational cost. Following standard procedures, we treat fluid-membrane interactions by distributing the membrane force onto nearby Eulerian grids. On rigid walls, we adopt the direct forcing method to enforce the nonslip boundary condition (44).

The geometric parameters are chosen to approximate the filtration experiment of Yap and Kamm (9): $L_x = 80\ \mu m$, $L_y = 20\ \mu m$, $w = 5\ \mu m$, and $L_c = 10\ \mu m$. The length of the wide channel upstream of the constriction is 2L_c, and that downstream is 5L_c. At the start of the simulation, the neutrophil is a circle of diameter $d = 10\ \mu m$ (1,2), with its center 0.8d ahead of the entry into the constriction. The physical and kinetic parameters of the model are summarized in Table 1, with literature sources given (37,45–50) where available. Note that some of the kinetic rate constants have no measured values. We have also assumed equal viscosity for the cytosol and the surrounding fluid, despite large viscosity ratios in reality (51). The rationale for choosing the parameter values is explained in the Supporting Material. Using these parameters, the Reynolds number is ~10^{-7}, but the inertial term is retained in the momentum equation. A capillary number defined using the rest-state cortical tension ranges from 0.0195 to 0.078 in our simulations.

To validate the flow solver, we have simulated the steady tank-treading of a capsule in a shear flow and compared the results with those in Sui et al. (52). The computational domain is a square box of sides H with the capsule at the center. We have varied the Eulerian grid size h as well as the membrane resolution l_0 in the following three test cases: 1) $h = H/128$ and $l_0 = 1.4h$; 2) $h = H/256$ and $l_0 = 2.8h$; and 3) $h = H/256$ and $l_0 = 1.4h$. The results of all three cases, for two capillary numbers, agree with those of Sui et al. (52) within 2%. Furthermore, we have tested the membrane resolution for the transit of a neutrophil through the constriction of Fig. 1, using the model parameters given above. With $h = L_y/128$ fixed, a coarse membrane resolution ($l_0 = 5.6h$) and a fine one ($l_0 = 2.8h$) predict transients in the neutrophil deformation that are virtually indistinguishable from each other. As a final validation, we have simulated the passage of a vesicle through a channel with a 2:1 contraction, with physical parameters matched to those of Le et al. (53) and grid size $h = L_y/128$ and $l_0 = 2.8h$. The trajectory of the vesicle agrees with that of Le et al. (53) to within 5%, and the vesicle shape is virtually indistinguishable from the snapshots of their Fig. 20. All subsequent results are generated using $h = L_y/128$ and $l_0 = 2.8h$, the latter corresponding to $N = 72$.
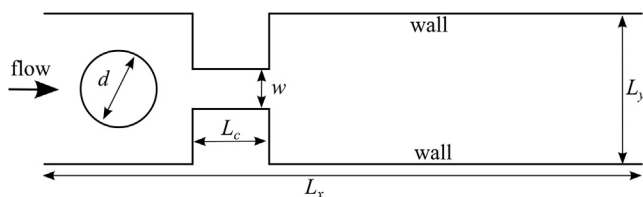

FIGURE 1   Geometry of the computational domain.

TABLE 1   Physical and kinetic parameters of the model

Symbol	Meaning	Value and References
η	cytosol and fluid viscosity	0.5 Pa × s
ρ	cytosol and fluid density	1000 kg/m³
ΔP	pressure drop	25–100 Pa (8,9)
ε_0	prestrain	0.1 (37,45)
E_c^0	cortical modulus	500 μN/m (4,46,47)
E_m	membrane modulus	500 μN/m (8)
k	coefficient in prestrain	1.5
k_b	bending modulus	9.2×10^{-17} J (48)
β	critical bending rate	10 s^{-1}
k_{pro}	protrusion coefficient	8 pN (30,49)
D	diffusivity	0.5 μm²/s (16,50)
k_{poly}	actin polymerization rate	0.02 s^{-1} (9)
γ	parameter in Rac activation	1–10 s^{-1} (15)
K	parameter in Rac activation	0.0187 μm^{-1}

The kinetic rates k_{on}, k_{off}, and k_τ will be varied in proportional to γ, as explained in the Supporting Material.

RESULTS AND DISCUSSION

In their experiments, Yap and Kamm (8,9) observed two major episodes during the neutrophil's passage through a narrow channel or filter: fluidization and activation. Activation, with protrusion of pseudopods, is necessarily preceded by polarization of the key signal proteins, especially Rac and RhoA. Accordingly, we divide our presentation below into three subsections on fluidization, polarization, and activation of the neutrophil.

Yap and Kamm (9) observed that the neutrophils were activated under a slow filtration rate but not under a faster filtration rate. They hypothesized that the slow filtration rate might have allowed the cell more time to develop polarity in the signaling proteins. In our simulation, however, varying the pressure drop ΔP would change the timescales for cell entry and passage, as well as the flow rate and membrane bending rate, the latter affecting cell fluidization. These simultaneous changes complicate the task of analyzing the competition between the timescale of cell entry and the kinetic timescale. Thus, we have adopted the simpler scheme of varying the kinetic rate for a constant flow rate. More specifically, we fix the ratios among the kinetic rate constants, and use γ to represent the chemical kinetic rates. Most of the results reported are for $\Delta P = 50$ Pa at two γ-values, $\gamma = 2.5$ s^{-1} for slow kinetics and $\gamma = 5$ s^{-1} for fast kinetics. An exception is Fig. 5, which covers a range of ΔP and γ-values. Movies S1 and S2 in the Supporting Material show representative solutions.

Fluidization

Fig. 2 illustrates the transit of the cell through the channel for the fast kinetics with $\gamma = 5$ s^{-1}. As the cell front deforms and enters the channel, the cortex starts to disassemble at the front first ($t = 1.54$ s), with the local modulus dropping below 20% of the resting value. After the cell has fully
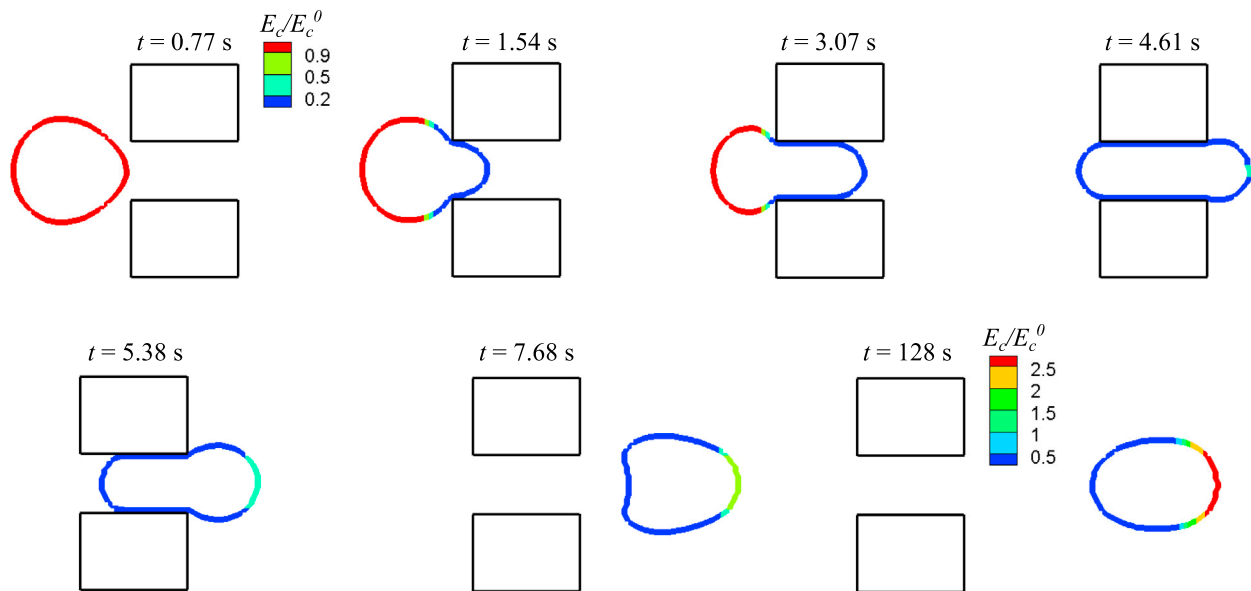
FIGURE 2 Passage of the neutrophil through the narrow channel for $\gamma = 5$ s^{-1}, depicted by snapshots taken at the times indicated in the plot. (*Colors*) Cortical modulus E_c scaled by its initial value for the resting state E_c^0. The first color bar applies to all frames except the last. To see this figure in color, go online.

entered the channel, the cortex has disassembled over the entire cell ($t = 4.61$ s). This corresponds to the experimentally observed fluidization. A more careful inspection shows that the fluidization proceeds with a melting front propagating from the front toward the rear of the cell as it enters the narrow channel. In the reference frame of the channel, however, the melting point stays more or less fixed in space, a small distance upstream of the entrance of the narrow channel. The salient corners of the entry bend the cell membrane at a rate that exceeds the threshold for cytoskeletal disassembly (Eq. 15).

Later, the cortex starts to grow back at the front; the recovery of the cytoskeleton is modulated by the active Rac according to Eq. 16. Eventually, E_c exceeds its resting value by nearly three times at the front of the cell (Fig. 2, $t = 128$ s). This corresponds to activation of the neutrophil, and will be discussed further in Activation. A similar scenario of fluidization occurs for the slow kinetics with $\gamma = 2.5$ s^{-1} (results not shown). This is consistent with the experimental observation that the kinetic rates have little effect on the fluidization of the cell or the mechanics of its transit (8). In our model, this is expected of course, as the criterion for cortical disassembly is based on the instantaneous rate of bending (Eq. 15).

In Fig. 2, the cell entry time is $t_e = 4.58$ s, but the timescale of bending appears to be much shorter, at <1 s. As cortical remodeling through actin turnover typically takes tens of seconds (54), it is reasonable that fluidization occurs in this case. To mimic the filtration experiments (9) with $t_e = 2$–15 s, we have varied ΔP to produce t_e between 2.15 and 11.6 s. Fluidization occurs in all these simulations and experiments, as expected.

Polarization

It is well known that pseudopods form because of actin polymerization and cortical reinforcement, which are regulated by the Rho GTPases Rac (13). Thus, we need to investigate the polarization of signaling proteins before neutrophil activation.

Fig. 3 shows the development of the Rac polarity for $\gamma = 5$ s^{-1}. Before the cell enters the channel ($t = 0.77$ s), a has a uniform distribution on the membrane: $a_0 = 2.67 \times 10^{-3}$ μm^{-1}. Once the cell enters, the deformation initially causes disassembly of the cortex network at the cell front. This relieves the cortical tension that inhibits Rac on the membrane (see Eq. 12), and so the level of active Rac a rises at the front of the cell ($t = 1.54$ s). By the time the cell is mostly inside the channel ($t = 4.61$ s), a has developed a maximum at the front tip, where it has had more time to grow than in the rear. However, the high a prompts the recovery of the local cytoskeleton (Fig. 2, $t = 5.38$ s), and thus the local cortical tension σ_τ (Eq. 2). The latter tends to suppress the local a through the FLNa-FilGap pathway (Eq. 10). The final outcome depends on γ, among other factors. For $\gamma = 5$ s^{-1}, a at the cell front surpasses a critical value, and a wave-pinning mechanism amplifies a to a high value and sustains a polarized a distribution long after the cell exits the channel (Fig. 3, $t = 128$ s). The polarity of a produces a large protrusion force at the cell front and serves as a precursor to cell activation. Conversely, for $\gamma = 2.5$ s^{-1}, the high a at the cell front disappears quickly after the cell exits the narrow channel and returns to a round shape (results not shown). A uniform distribution of a obtains, and the cell is neither polarized nor activated.
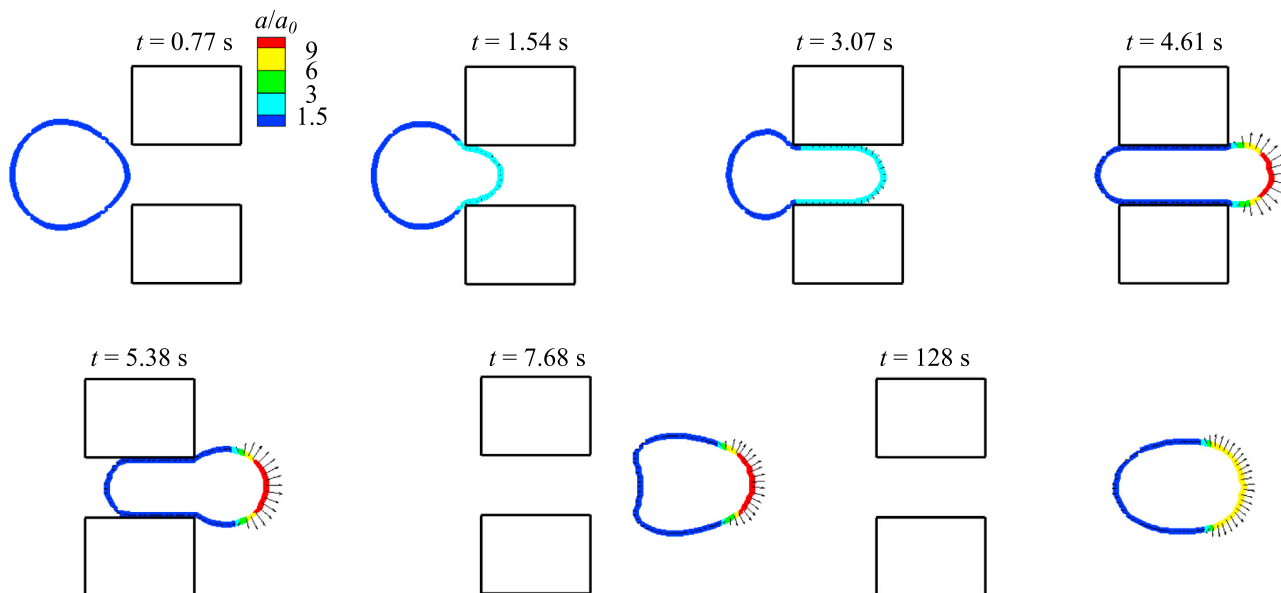
FIGURE 3   Passage of the neutrophil through the narrow channel for $\gamma = 5$ s^{-1}. (*Colors*) Level of active Rac a on the membrane. (*Arrows*) Protrusion force F_{pro}, with a maximum of 73.4 pN at the front node and a force density of 168 pN/μm at $t = 128$ s. To see this figure in color, go online.

For a more quantitative analysis, Fig. 4 compares the temporal evolutions of a at the cell's front tip (denoted by a_f) and the back tip (a_b). For the nonpolarized case at $\gamma = 2.5$ s^{-1} (Fig. 4 a), a has a uniform distribution, with $a_f = a_b$, before any part of the cortex has fluidized ($t < 1.18$ s). Afterwards, the onset of cortical fluidization at the cell front removes the cortical tension there and allows a_f to rise. This trend continues until $t = 4.3$ s, when a_f peaks before starting to decline. This reflects the feedback between Rac and the cytoskeleton. The higher a_f induces cortical reconstitution, which produces a cortical tension that inhibits a_f through the FLNa-FilGAP pathway. Rac at the rear a_b follows qualitatively the same behavior, but with a delay of ~3 s relative to that of a_f. This is because the rear fluidizes later than the front. Both a_f and a_b compete for the pool of inactive I in the cytosol. Thus, when a_f starts to rise at $t = 1.18$ s, the cytosolic Rac level I drops, and this causes a mild dip in a_b. Similarly, as a_b starts to rise, that reduces I and contributes to the rapid decline of a_f starting from $t = 4.3$ s. Later, both a_b and a_f relax to the equilibrium value in ~150 s (long-term relaxation not shown in Fig. 4). Thus, the cell shows no long-term polarity.

In contrast, the high kinetic rate $\gamma = 5$ s^{-1} produces strong polarization in Fig. 4 b. Because of the fast chemical rates, a_f rises sharply and depletes I quickly. By the time the rear end fluidizes ($t = 4.61$ s), there remains little inactive Rac in the cytosol to feed the growth of a_b. Thus a_b stays low. However, a_f continues to rise thanks to k_+ of Eq. 9. Subsequently, a wave-pinning mechanism keeps a_f at the high level and a_b at the low level. The polarized state persists with no sign of decay until the end of the simulation ($t = 200$ s). The wave-pinning mechanism is discussed further in the Supporting Material.

Polarization is not only affected by the kinetic rate γ but also by the entry time t_e of the neutrophil. Indeed the experimental protocol of Yap and Kamm (8,9) was to vary the pressure drop ΔP and hence the entry time of the neutrophil, from 0.1 to 10 s in the microfluidic channel (8), and from 2 to 15 s in filtration (9). As t_e determines how much time is available for Rac to polarize, its role is not unexpected. To vary t_e, we have simulated four different Δp-values: 25, 50, 75, and 100 Pa, which produce the following range of entry times for the γ-values tested: 2.15 s $\leq t_e \leq$ 11.6 s. The results are depicted by the phase diagrams of Fig. 5, with two regimes: nonpolarization for slow kinetics and/or fast flow, and polarization for fast kinetics and/or slow flow.

The fact that the critical γ required for polarization increases with flow rate (Fig. 5 a) suggests a criterion based on γt_e, which may be viewed as the amount of Rac activated within the cell entry time. Thus, we can recast the phase diagram into Fig. 5 b. Although the boundary is not horizontal, qualitatively this supports the argument of Yap and Kamm (9) that polarization is the outcome of the competition between two timescales. If the chemical time γ^{-1} is much shorter than the entry time t_e, Rac has sufficient time to develop at the front of the cell, and polarization occurs. Otherwise, Rac does not have time to develop a sufficient front-rear difference before the cell exits the narrow channel, and polarization does not occur.

It is tempting to check the above criterion against experimental data. Unfortunately, our γ-parameter appears in a highly specific algebraic form in the Rac evolution equation (Eq. 12), and there is no experimental measurement of it. Nevertheless, a rough estimation can be made
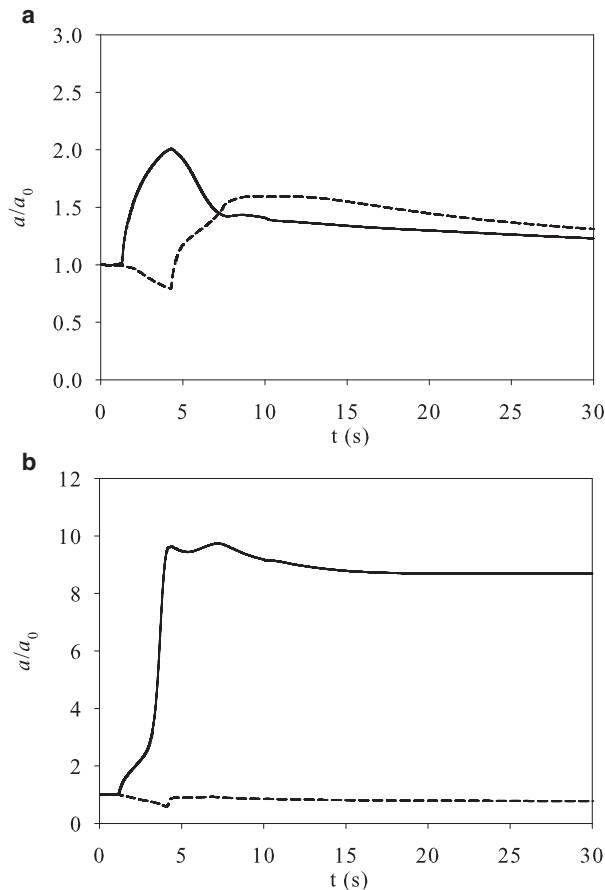
FIGURE 4 Evolution of active Rac at the cell's front tip (a_f, *solid line*) and back tip (a_b, *dashed line*). (*a*) The nonpolarized case at the slow kinetic rate $\gamma = 2.5$ s^{-1}; (*b*) the polarized case at $\gamma = 5$ s^{-1}.
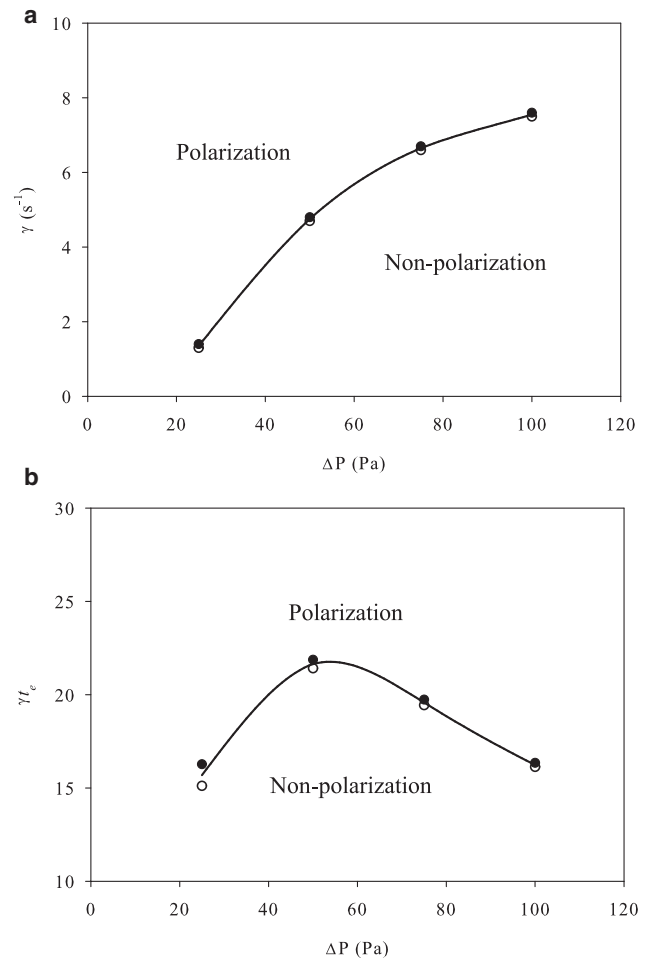

FIGURE 5 Phase diagram showing critical conditions for neutrophil polarization, in the parameter space of (*a*) ΔP versus t_e, and (*b*) ΔP versus γt_e. (*Solid circles*) Polarization; (*open circles*) nonpolarization. The boundary is drawn between the two.

based on the decay of fluorescent Rac spots on the membrane (15): $\gamma \sim 2$ s^{-1} (see the Supporting Material for details). In the experiment of Yap and Kamm (9), an entry time of $t_e = 2$ s (fast filtration) does not cause polarization but $t_e = 15$ s (slow filtration) does. Thus, one can estimate a critical value of γt_e between 4 and 30. This is consistent with the predicted boundary in Fig. 5 *b*.

Activation

Experimentally, neutrophil activation has been characterized by two quantities (8,9): cell morphology with the protrusion of pseudopods, and polarized distribution of F-actin with enriched cortex inside the pseudopods. We will examine these in our numerical simulations. First, we define a deformation index (DI) to reflect the deviation of cell shape from its original circular shape,

$$\mathrm{DI} = \sqrt{\frac{\sum_{i=1}^{N}(2r_i - d)^2}{Nd^2}}, \qquad (17)$$

where r_i is the distance of the ith node from the centroid of the cell. Fig. 6 shows the evolution of the DI at the two kinetic rates examined before, $\gamma = 2.5$ s^{-1} and $\gamma = 5$ s^{-1}. In both cases, DI initially rises sharply and reaches a maximum of ~0.4 at $t = 4.6$ s. This corresponds to the point of maximum deformation of the neutrophil inside the narrow channel. So far, γ has exerted little influence as DI has mostly been determined by the hydrodynamics and wall confinement. After that, DI declines as the cell exits the channel and starts to retract under membrane elasticity. For the slow kinetic rate, the Rac signal relaxes toward a uniform distribution. Thus, DI approaches zero at $t \approx 20$ s, indicating recovery of the cell to its initial circular shape. Yap and Kamm (9) reported a similar process of recovery for nonactivated neutrophil, but over a longer timescale (~100 s). For the fast kinetic rate, the protrusion force sustains a finite cell deformation with $DI = 0.12$ against elastic relaxation, even after the neutrophil has
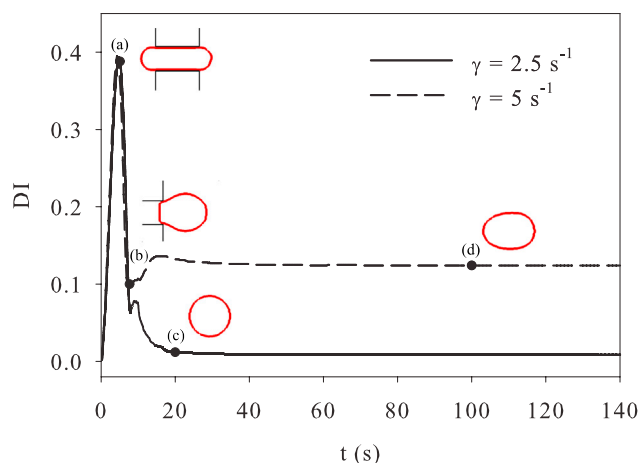
FIGURE 6 Evolution of the cell deformation index (*DI*) for the slow kinetic rate $\gamma = 2.5$ s^{-1} and the fast rate $\gamma = 5$ s^{-1}. The snapshots (*a–d*) show the cell shapes at four times (marked by *black dots* on the *curves*). To see this figure in color, go online.

long exited the narrow channel. The polarized Rac distribution and cell shape reach a steady state at t ~ 80 s. This is our equivalent of a protruding pseudopod.

It is interesting to compare the neutrophil activation predicted by the model with experimental observation. Yap and Kamm (9) found that after gentle filtering at low speed or pressure drop, the neutrophil is activated and forms pseudopods, where F-actin is highly concentrated (Fig. 7, *b–d*). In the activated state, however, experimental images show considerable variation in the shape and size of the pseudopods, ranging from small bumps on the cell edge (*d*) to wider, more distributed F-actin covering approximately half of the cell periphery (*b* and *c*). These can be compared with the activated state in our simulations. If we take the front of the cell bearing large E_c in Fig. 2 (*t* = 128 s), or equivalently large *a* and F_{pro} in Fig. 3, to be the pseudopod, then its broad and smooth shape resembles Fig. 7 *c* much more than the pointed pseudopods of Fig. 7 *d*. Possibly, the simple 2D representation of the cell membrane and the assumption of a spatially uniform *I* have deprived the model of an ability to capture smaller-scale spatial variations on the membrane.

The fluidization, polarization, and activation sequence can also be viewed from the temporal evolution of the cortical modulus at the front and the back of the cell (Fig. 8). For both the polarized and nonpolarized cases,
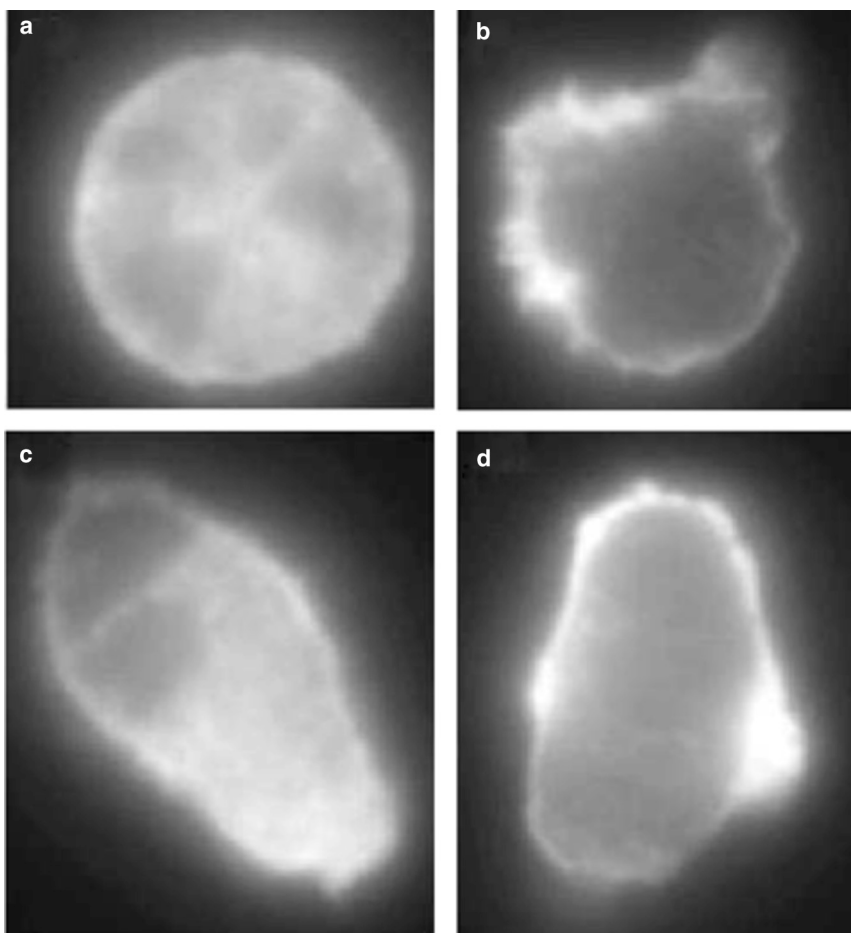

FIGURE 7 Distribution of F-actin inside neutrophils before and after passing through 3 μm pores in a filter. The cells are stained with tetramethylrhodamine isothiocyanate-phalloidin to show F-actin concentration. (*a*) The resting neutrophil before filtration. (*b*) Activated neutrophil filtered under a constant pressure drop. (*c* and *d*) Activated neutrophil filtered under a constant flow rate. (Adapted from Yap and Kamm (9) with permission; ©the American Physiological Society.)
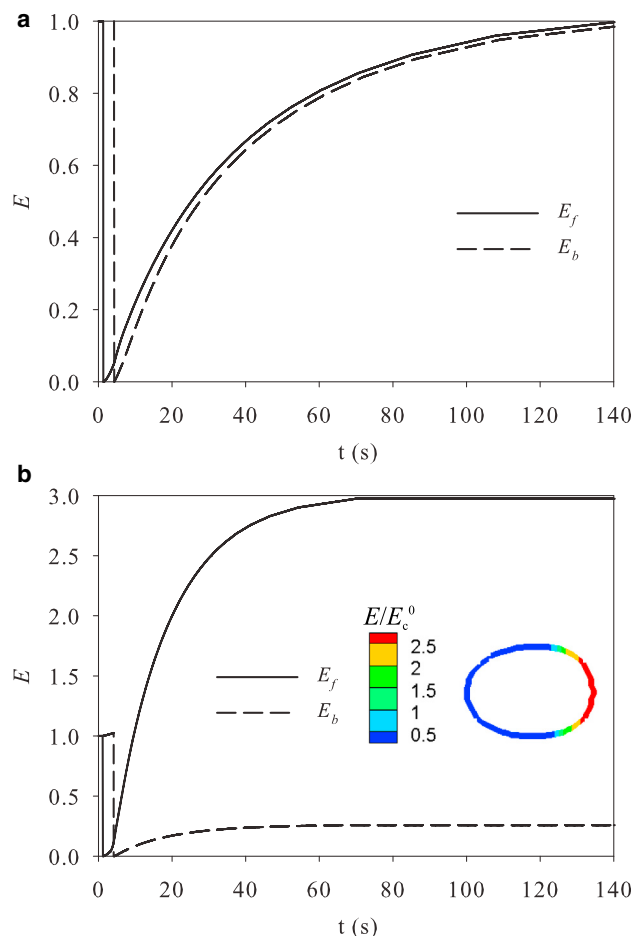
FIGURE 8 Temporal evolution of the cortical modulus at the front tip (E_f) and the rear tip (E_b) of the cell, normalized by the resting state modulus E_c^0. (a) The nonpolarized case at $\gamma = 2.5$ s^{-1}. (b) The polarized and activated case at $\gamma = 5$ s^{-1}, with the inset, taken from Fig. 2 at $t = 128$ s, depicting the steady-state, activated cell. To see this figure in color, go online.

the initial dip in the cortical modulus E_c indicates fluidization. The rear fluidizes some 3 s after the front does, reflecting the entry of the cell body into the narrow channel. For the nonpolarized case ($\gamma = 2.5$ s^{-1}), the cortical elasticity grows back more or less uniformly afterwards, thanks to the even distribution of the active Rac on the membrane. The recovery takes some 140 s to complete, long after the cell shape has returned to circular (Fig. 8 a). Experimentally, Yap and Kamm (9) reported that for the nonactivated case, the F-actin recovers to its initial level in ~120 s. This apparent agreement of the recovery time is achieved by tuning the polymerization rate to $k_{poly} = 0.02$ s^{-1}. For the polarized and activated case ($\gamma = 5$ s^{-1}), on the other hand, the cortical elasticity grows back nonuniformly. At the cell front, E_f rises much more rapidly than E_b at the cell back, and stabilizes at a much higher level (Fig. 8 b). This is due to the polarized Rac distribution in the activated case. In the steady state, achieved at t ~ 80 s and depicted by the inset, the high cortical modulus at the front corresponds

to the high F-actin content inside pseudopods that has been documented experimentally (9).

CONCLUSIONS

In this article, we have proposed a chemo-mechanical model for neutrophil activation in response to mechanical deformation, and simulated the fluidization, polarization, and activation of a neutrophil as it traverses a narrow channel. The model integrates insights and hypotheses from previous experiments into a coherent theoretical framework, and predicts the salient features of how a neutrophil senses mechanical stimulation and responds by remodeling its cortex. We may summarize the model predictions as follows:

Fluidization

As the neutrophil deforms and enters a narrow channel, its cytoskeleton starts to melt at the cell front where it sustains severe mechanical deformation. The melting front propagates toward the rear of the cell, and by the time the bulk of the cell is inside the channel, the entire cytoskeleton has fluidized.

Polarization

Melting of the cytoskeleton eliminates the cortical tension that inhibits Rac activity on the membrane. Thus, inactive Rac in the cytosol becomes active Rac on the membrane. If the kinetic rate of Rac turnover is high relative to the reciprocal of the entry time, a polarized Rac distribution prevails by a wave-pinning mechanism even after the cell exits the confining channel.

Activation

The polarized Rac distribution induces a protrusion at the cell front, where the cortex also becomes highly enriched. Thus the neutrophil becomes activated.

The model captures the main features of the experiment from a set of reasonable assumptions about the chemical kinetics, signaling pathways, and hydrodynamics. In particular, the results have confirmed the hypothesis (8,9) that neutrophil activation depends on the competition of two timescales. If the kinetic time is much shorter than the cell entry time, Rac builds up a sufficient front-rear difference before the cell exits, and polarization and activation ensue. If the kinetic time is too long, the cell exits with a weak front-rear differential in Rac, which decays subsequently. No polarization or activation occurs and the cell simply returns to its spherical inactive state. Based on this competition, we have constructed a phase diagram from numerical data, and the critical condition for cell activation is consistent with experimental observations. The shape of the activated cell and the polarized distributions of Rac, cortical

modulus, and protrusion force also agree qualitatively with experiments.

Of necessity the model introduces various simplifications, and these may have limited its ability to capture finer features of the real process. For example, the predicted pseudopod consists of a broad frontal portion of the cell, whereas in reality, pseudopods sometimes take on smaller dimensions and varied shapes and locations. The model simplifications fall into two categories, mechanical and chemical. Mechanically we model the cell in 2D, and represent the plasma membrane and the underlying cortex using a single mechanical element: elastic segments along the cell's outline. As such, we neglect the details of cortex breakage and destruction, and indicate the cortical integrity only by the cortical modulus. Moreover, the cytosol is assigned the same viscosity as the outside fluid. This simplifies the immersed-boundary formalism and facilitates the computation. In treating the chemical kinetics of polarization, we have neglected the intricate relationship among Rho GTPases, and instead used a single protein, Rac, to describe the polarization process. Because of this, the inhibition of membrane Rac by cortical tension, the promotion of cortical growth by Rac, and the development of a protrusion force are all modeled ad hoc.

These assumptions and simplifications can be viewed as motivations for future work. For example, the model suggests future experiments to measure protein and force distributions with spatial resolution during neutrophil activation. Such data can be used to validate the model predictions of polarization and pseudopod protrusion. Furthermore, they may provide insights into how the cortical tension inhibits Rac, and how Rac and Rho produce protrusion and contraction forces in return. With a deeper understanding of the interaction between signaling proteins and mechanical forces, one can refine and generalize the theoretical model for mechanically induced neutrophil activation.

SUPPORTING MATERIAL

Supporting Materials and Methods, one figure, and two movies are available at http://www.biophysj.org/biophysj/supplemental/S0006-3495(15)01107-8.

AUTHOR CONTRIBUTIONS

J.J.F. designed the research; T.W. wrote the code and carried out the simulations; and T.W. and J.J.F. analyzed the data and wrote the article.

ACKNOWLEDGMENTS

SUPPORTING CITATIONS

Reference (55) appears in the Supporting Material.

REFERENCES

1. Ting-Beall, H. P., D. Needham, and R. M. Hochmuth. 1993. Volume and osmotic properties of human neutrophils. *Blood.* 81:2774–2780.

2. Young, B., J. S. Lowe, …, J. W. Heath. 2006. Wheaters' Functional Histology: A Text and Color Atlas, 5th Ed. Churchill Livingstone, London, UK.

3. Kolaczkowska, E., and P. Kubes. 2013. Neutrophil recruitment and function in health and inflammation. *Nat. Rev. Immunol.* 13:159–175.

4. Zhelev, D. V., and R. M. Hochmuth. 1995. Mechanically stimulated cytoskeleton rearrangement and cortical contraction in human neutrophils. *Biophys. J.* 68:2004–2014.

5. Moazzam, F., F. A. DeLano, …, G. W. Schmid-Schönbein. 1997. The leukocyte response to fluid stress. *Proc. Natl. Acad. Sci. USA.* 94:5338–5343.

6. Coughlin, M. F., and G. W. Schmid-Schönbein. 2004. Pseudopod projection and cell spreading of passive leukocytes in response to fluid shear stress. *Biophys. J.* 87:2035–2042.

7. Makino, A., M. Glogauer, …, G. W. Schmid-Schönbein. 2005. Control of neutrophil pseudopods by fluid shear: role of Rho family GTPases. *Am. J. Physiol. Cell Physiol.* 288:C863–C871.

8. Yap, B., and R. D. Kamm. 2005. Mechanical deformation of neutrophils into narrow channels induces pseudopod projection and changes in biomechanical properties. *J. Appl. Physiol.* 98:1930–1939.

9. Yap, B., and R. D. Kamm. 2005. Cytoskeletal remodeling and cellular activation during deformation of neutrophils into narrow channels. *J. Appl. Physiol.* 99:2323–2330.

10. Shifrin, Y., P. D. Arora, …, C. A. McCulloch. 2009. The role of FilGAP-filamin A interactions in mechanoprotection. *Mol. Biol. Cell.* 20:1269–1279.

11. Ehrlicher, A. J., F. Nakamura, …, T. P. Stossel. 2011. Mechanical strain in actin networks regulates FilGAP and integrin binding to filamin A. *Nature.* 478:260–263.

12. Houk, A. R., A. Jilkine, …, O. D. Weiner. 2012. Membrane tension maintains cell polarity by confining signals to the leading edge during neutrophil migration. *Cell.* 148:175–188.

13. Hall, A. 1998. Rho GTPases and the actin cytoskeleton. *Science.* 279:509–514.

14. Olofsson, B. 1999. Rho guanine dissociation inhibitors: pivotal molecules in cellular signalling. *Cell. Signal.* 11:545–554.

15. Sako, Y., K. Hibino, …, T. Yanagida. 2000. Single-molecule imaging of signaling molecules in living cells. *Single Mol.* 1:159–163.

16. Postma, M., L. Bosgraaf, …, P. J. M. van Haastert. 2004. Chemotaxis: signalling modules join hands at front and tail. *EMBO Rep.* 5:35–40.

17. Mohandas, N., and E. Evans. 1994. Mechanical properties of the red cell membrane in relation to molecular structure and genetic defects. *Annu. Rev. Biophys. Biomol. Struct.* 23:787–818.

18. Pasternak, C., J. A. Spudich, and E. L. Elson. 1989. Capping of surface receptors and concomitant cortical tension are generated by conventional myosin. *Nature.* 341:549–551.

19. Egelhoff, T. T., T. V. Naismith, and F. V. Brozovich. 1996. Myosin-based cortical tension in *Dictyostelium* resolved into heavy and light chain-regulated components. *J. Muscle Res. Cell Motil.* 17:269–274.

20. Kimura, K., M. Ito, …, K. Kaibuchi. 1996. Regulation of myosin phosphatase by Rho and Rho-associated kinase (Rho-kinase). *Science.* 273:245–248.

21. Wada, S., and R. Kobayashi. 2003. Numerical simulation of various shape changes of a swollen red blood cell by decrease of its volume. *Trans. Jpn. Soc. Mech. Eng.* 69:14–21.

22. Tsubota, K. I., and S. Wada. 2010. Elastic force of red blood cell membrane during tank-treading motion: consideration of the membrane's natural state. *Int. J. Mech. Sci.* 52:356–364.

23. Wu, T., and J. J. Feng. 2013. Simulation of malaria-infected red blood cells in microfluidic channels: passage and blockage. *Biomicrofluidics.* 7:44115.

24. Discher, D. E., D. H. Boal, and S. K. Boey. 1998. Simulations of the erythrocyte cytoskeleton at large deformation. II. Micropipette aspiration. *Biophys. J.* 75:1584–1597.

25. Fedosov, D. A., B. Caswell, …, G. E. Karniadakis. 2011. Quantifying the biophysical characteristics of *Plasmodium-falciparum*-parasitized red blood cells in microcirculation. *Proc. Natl. Acad. Sci. USA.* 108:35–39.

26. Dong, C., and R. Skalak. 1992. Leukocyte deformability: finite element modeling of large viscoelastic deformation. *J. Theor. Biol.* 158:173–193.

27. Marella, S. V., and H. S. Udaykumar. 2004. Computational analysis of the deformability of leukocytes modeled with viscous and elastic structural components. *Phys. Fluids.* 16:244–264.

28. Leong, F. Y., Q. Li, …, K.-H. Chiam. 2011. Modeling cell entry into a micro-channel. *Biomech. Model. Mechanobiol.* 10:755–766.

29. Yoo, S. K., Q. Deng, …, A. Huttenlocher. 2010. Differential regulation of protrusion and polarity by PI3K during neutrophil motility in live zebrafish. *Dev. Cell.* 18:226–236.

30. Vanderlei, B., J. J. Feng, and L. Edelstein-Keshet. 2011. A computational model of cell polarization and motility coupling mechanics and biochemistry. *Multiscale Model. Simul.* 9:1420–1443.

31. Holmes, W. R., B. Lin, …, L. Edelstein-Keshet. 2012. Modelling cell polarization driven by synthetic spatially graded Rac activation. *PLOS Comput. Biol.* 8:e1002366.

32. Lin, B., W. R. Holmes, …, A. Levchenko. 2012. Synthetic spatially graded Rac activation drives cell polarization and movement. *Proc. Natl. Acad. Sci. USA.* 109:E3668–E3677.

33. Marée, A. F. M., A. Jilkine, …, L. Edelstein-Keshet. 2006. Polarization and movement of keratocytes: a multiscale modelling approach. *Bull. Math. Biol.* 68:1169–1211.

34. Mori, Y., A. Jilkine, and L. Edelstein-Keshet. 2008. Wave-pinning and cell polarity from a bistable reaction-diffusion system. *Biophys. J.* 94:3684–3697.

35. Mori, Y., A. Jilkine, and L. Edelstein-Keshet. 2011. Asymptotic and bifurcation analysis of wave-pinning in a reaction-diffusion model for cell polarization. *SIAM J. Appl. Math.* 71:1401–1427.

36. Wong, K., O. Pertz, …, H. Bourne. 2006. Neutrophil polarization: spatiotemporal dynamics of RhoA activity support a self-organizing mechanism. *Proc. Natl. Acad. Sci. USA.* 103:3639–3644.

37. Costa, K. D., W. J. Hucker, and F. C. P. Yin. 2002. Buckling of actin stress fibers: a new wrinkle in the cytoskeletal tapestry. *Cell Motil. Cytoskeleton.* 52:266–274.

38. Sato, K., T. Adachi, …, Y. Tomita. 2005. Quantitative evaluation of threshold fiber strain that induces reorganization of cytoskeletal actin fiber structure in osteoblastic cells. *J. Biomech.* 38:1895–1901.

39. Murrell, M. P., and M. L. Gardel. 2012. F-actin buckling coordinates contractility and severing in a biomimetic actomyosin cortex. *Proc. Natl. Acad. Sci. USA.* 109:20820–20825.

40. Alvarado, J., M. Sheinman, …, G. H. Koenderink. 2013. Molecular motors robustly drive active gels to a critically connected state. *Nat. Phys.* 9:591–597.

41. Machesky, L. M., and A. Hall. 1997. Role of actin polymerization and adhesion to extracellular matrix in Rac- and Rho-induced cytoskeletal reorganization. *J. Cell Biol.* 138:913–926.

42. Peskin, C. S. 2002. The immersed boundary methods. *Acta Numer.* 11:479–517.

43. Yu, Z., X. Shao, and A. Wachs. 2006. A fictitious domain method for particulate flows with heat transfer. *J. Comput. Phys.* 217:424–452.

44. Fadlun, E. A., R. Verzicco, …, J. Mohd-Yusof. 2000. Combined immersed-boundary finite-difference methods for three-dimensional complex flow simulations. *J. Comput. Phys.* 161:35–60.

45. Lu, L., Y. Feng, …, F. C. P. Yin. 2008. Actin stress fiber pre-extension in human aortic endothelial cells. *Cell Motil. Cytoskeleton.* 65:281–294.

46. Hochmuth, R. M. 2000. Micropipette aspiration of living cells. *J. Biomech.* 33:15–22.

47. Herant, M., V. Heinrich, and M. Dembo. 2005. Mechanics of neutrophil phagocytosis: behavior of the cortical tension. *J. Cell Sci.* 118:1789–1797.

48. Zhelev, D. V., D. Needham, and R. M. Hochmuth. 1994. A novel micropipet method for measuring the bending modulus of vesicle membranes. *Biophys. J.* 67:720–727.

49. Prass, M., K. Jacobson, …, M. Radmacher. 2006. Direct measurement of the lamellipodial protrusive force in a migrating cell. *J. Cell Biol.* 174:767–772.

50. Cowan, A. E., L. Nakhimovsky, …, D. E. Koppel. 1997. Barriers to diffusion of plasma membrane proteins form early during guinea pig spermiogenesis. *Biophys. J.* 73:507–516.

51. Tsai, M. A., R. S. Frank, and R. E. Waugh. 1993. Passive mechanical behavior of human neutrophils: power-law fluid. *Biophys. J.* 65:2078–2088.

52. Sui, Y., Y. T. Chew, …, H. T. Low. 2007. Transient deformation of elastic capsules in shear flow: effect of membrane bending stiffness. *Phys. Rev. E Stat. Nonlin. Soft Matter Phys.* 75:066301.

53. Le, D. V., B. C. Khoo, and J. Peraire. 2006. An immersed interface method for viscous incompressible flows involving rigid and flexible boundaries. *J. Comput. Phys.* 220:109–138.

54. Fritzsche, M., A. Lewalle, …, G. Charras. 2013. Analysis of turnover dynamics of the submembranous actin cortex. *Mol. Biol. Cell.* 24:757–767.

55. Prosperetti, A., and G. Tryggvason. 2007. Computational Methods for Multiphase Flow. Cambridge University Press, Cambridge, UK.

Modeling the mechanosensitivity of neutrophils passing through a narrow channel (Supporting Material)

Tenghu Wu

Department of Chemical and Biological Engineering,
University of British Columbia, Vancouver, BC V6T 1Z3, Canada

James J. Feng*

Department of Chemical and Biological Engineering,
University of British Columbia, Vancouver, BC V6T 1Z3, Canada, and
Department of Mathematics,
University of British Columbia, Vancouver, BC V6T 1Z2, Canada

1   Model parameters

Of the physical and kinetic parameters listed in Table 1, some are taken directly from literature sources, others are estimated from literature data, and still others are chosen to save computational cost or to produce reasonable predictions. The latter two cases are explained in the following.

The viscosity ratio between the cell cytoplasm and the surrounding fluid is set to be 1, and the viscosity is chosen to be $\eta = 0.5$ Pa·s. In reality, the cytoplasmic viscosity of neutrophils is shear-thinning, and on the order of 100 Pa·s (1). This is more than 10^4 times greater than that of the suspending medium, whose viscosity is typically comparable to that of water. Simulating such a large viscosity ratio is numerically challenging, if possible at all (2). Thus we have adopted the artificial viscosity value that is between those of the cytoplasm and the suspending fluid, such that for the range of pressure drop ΔP tested, the neutrophil will enter and pass through the narrow channel on time scales similar to those in the experiments of Yap and Kamm (3, 4). The pressure drop applied to push the cell through the constricting channel will be varied within the range $\Delta P = 25$ to 100 Pa to mimic the experimental conditions of Yap and Kamm (3, 4).

---

*Corresponding author. E-mail: james.feng@ubc.ca

The measured values of the rest-state cortical tension σ_0 range between 30 and 90 μN/m (5–7). Hence we set $\sigma_0 = 50$ μN/m for the neutrophil at rest. The pre-strain of the resting state ε_0 is chosen to be 0.1 according to the literature (8, 9). Now the cortical modulus in the resting state can be backed out: $E_c^0 = \sigma_0/\varepsilon_0 = 500$ μN/m. Note that in the cortical tension the plasma membrane contribution has been excluded. In the study of Yap and Kamm (3), the residual elastic modulus after the neutrophil fluidization is about 50% of the original one, which is mainly due to the plasma membrane. Thus we set the elastic modulus for the plasm membrane to be the same as that of the cortex $E_m = 500$ μN/m. The coefficient k appears in the dependence of the pre-strain ϵ on the local active Rac level a. Its value is chosen such that the cortical tension exerts sufficient inhibition on Rac activation in Eq. 12, which models the FLNa-FilGAP pathway.

The bending modulus k_b is chosen based on measured values (10), but a conversion is necessary. In the formulation of Zhelev et $al.$ (10), the bending energy of a circle is $\kappa \int C\,ds = 2\pi\kappa$, where κ is a bending constant and C is the local curvature. In our discretized model, however, the bending modulus k_b is defined between pairs of neighboring segments. Thus, the total bending energy of a discretized circle is $\Sigma\frac{k_b}{2}\tan^2\left(\frac{\Theta}{2}\right) \approx \frac{k_b\pi^2}{2N}$ for a large N, N being the number of segments in the circle. Equating the two gives our k_b value in terms of measured κ: $k_b = \frac{4N}{\pi}\kappa$. This yields the value cited in Table 1 for $N = 72$. The ratio between the bending and in-plane strain energy is on the order of 10^{-3}. Thus, bending plays a negligible role in the deformation and activation of the neutrophil.

The value of β is chosen such that the mild deformation of the cell in the wide part of the channel does not disrupt the cytoskeleton, but the severe deformation upon entering the narrow channel does. The protrusion coefficient k_{pro} is chosen after a previous model (11). With this value, the protrusion force density at the cell's front can be estimated as $(k_{pro}/l_0)(a/a_0) \sim 180$ pN/μm in our simulation. This is comparable to experimental values around 300 pN/μm (12). The diffusion rate D of active Rac on the membrane ranges from 0.1 to 0.5 μm^2/s (13, 14), and we use $D = 0.5$ μm^2/s.

In the simulation, we will explore a range of γ values while keeping these ratios of the rate constants fixed: $k_{on} : \gamma : k_{off} : k_\tau\sigma_0 = 0.05 : 1 : 2 : 0.4$. This strategy is informed by the fact that Eq. 12, if divided by γ on both sides, will contain the ratios of these kinetic rate constants on the right-hand side, with γ scaling the kinetic time scale on the left-hand side. The ratios are based on those used in an earlier model (15). To estimate the value of γ, we use the experiment of Sako et $al.$ (16) that measured the life-time

2

of individual spots of fluorescent Rac on the cell membrane. They found that more than 80% of the spots disappear within 1 s. This suggests a Rac off-rate k_{off} above 1 s^{-1}. As the Rac distribution is in equilibrium in the experiment, with attachment balanced by detachment, we can estimate the on-rate, and hence γ, to be above 1 s^{-1}. Thus, $\gamma = 2$ s^{-1} appears to be a reasonable estimation. In our simulations, we have tested the range $\gamma = 1$ s^{-1} to 10 s^{-1}, and presented mostly results for $\gamma = 2.5$ s^{-1} and $\gamma = 5$ s^{-1}. K is the saturation parameter (17, 18), and its value is chosen such that the system exhibits bistable solutions and the wave-pinning mechanism for polarization. Based on these parameters, the equilibrium Rac concentration on the membrane before cell deformation is $a_0 = 2.67 \times 10^{-3}$ μm^{-1}.

2 Wave-pinning

The wave-pinning mechanism generates polarization in a cell described by a reaction-diffusion system (17, 18). It can be appreciated by analyzing the steady-state solution of the kinetic equation governing a (Eq. 12). For simplicity, we may ignore for the moment the diffusion and inhibition of Rac by cortical tension in Eq. 12. The steady-state solution is thus given by this simplified equation:

$$\left(\frac{k_{on}}{\gamma} + \frac{a^2}{K^2 + a^2} \right) \frac{I}{d} - \frac{k_{off}}{\gamma} a = 0, \tag{S1}$$

where a is the local Rac level on the membrane, and I is taken for the moment to be a free parameter, unrelated to a. The steady-state solution $a(I)$ exhibits the prototypical shape of Fig. S1 that allows multiple states. Note that the nullcine is the same for the kinetic rates $\gamma = 2.5$ s^{-1} and 5 s^{-1}, since the ratios k_{on}/γ and k_{off}/γ are kept constant in our computations. If I is too small or too large, a single solution prevails, with a low a^- or high a^+, respectively. For the intermediate I values, however, two stable branches of the solution exist. If a perturbation pushes a past the threshold marked by the unstable solution, it will jump from the low branch to the higher branch (arrow from point 1) or vice versa (point 2).

In the actual computation, I and a are constrained by Rac conservation (Eq. 5); one decreases when the other increases. Thus, the trajectory of the solution typically starts from a large I and small a and goes toward the upper left. If a increases sufficiently to exceed the threshold, the solution proceeds to land on the upper branch. Otherwise it stays close to the lower branch and eventually loops back as the neutrophil exits the channel.
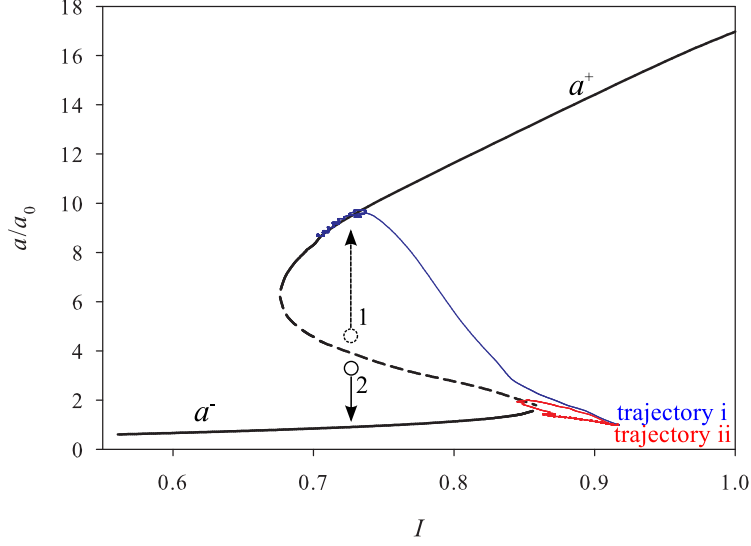
Figure S1: The nullcine for the simplified reaction-diffusion equation (Eq. S1). Trajectory (i) corresponds to a_f at the front tip of the polarizing cell ($\gamma = 5$ s^{-1}), while trajectory (ii) to a_f of the non-polarizing case ($\gamma = 2.5$ s^{-1}).

Figure S1 plots two trajectories that illustrate these behaviors. Trajectory (i), corresponding to a_f of the polarizing case (Fig. 4b), rises rapidly above the unstable branch as I shrinks, and winds up on the upper branch of the solution. Trajectory (ii), corresponding to the non-polarizing case (Fig. 4a), stays low and eventually loops back to its starting point, as the cell exits the narrow channel and recovers its resting state.

Moreover, a varies spatially, and its diffusion and inhibition by the changing cortical tension modify the simple picture above. The change of the cell circumference during the simulation also plays a role. In fact, a close inspection of trajectory (ii) in Fig. S1 shows that for a time it has climbed slightly above the unstable branch, only to be forced to cross it downward by the above factors that are not considered in the simplified Eq. S1. Despite such complications, the basic mechanism remains qualitatively the same. In particular, as the cortical fluidization propagates from the front toward the rear, so does the rise of the local a. Thus, the a solution exhibits a traveling wave pattern, with the high a^+ solution extending backward in time. This

4

continues until I becomes too low to keep raising a to the upper branch. The travelling wave becomes pinned, and a more or less steady polarized pattern obtains, with high a^+ at one end and low a^- at the other. This is the essence of the wave-pinning mechanism (17).

3   Online movies

Two online movies depict the entire process of the neutrophil's transit through the narrow channel, without activation at the lower kinetic rate ($\gamma = 2.5$ s^{-1}) and with activation at the higher one ($\gamma = 5$ s^{-1}). Following are the captions to the two movies.

Movie 1: Passage of the neutrophil through the narrow channel with initial fluidization but without polarization and activation. $\gamma = 2.5$ s^{-1} and $\Delta P = 50$ Pa. The color indicates the cortical modulus E_c scaled by the rest-state value E_c^0. The duration of the movie is 76.8 s in real time, and one unit length is 20 μm.

Movie 2: Passage of the neutrophil through the narrow channel with fluidization, polarization and activation. $\gamma = 5$ s^{-1} and $\Delta P = 50$ Pa. The color indicates the cortical modulus E_c scaled by the rest-state value E_c^0, and the arrows indicate the protrusion force. The duration of the movie is 64 s in real time, and one unit length is 20 μm.

References

1. Tsai, M. A., R. S. Frank, and R. E. Waugh, 1993. Passive mechanical behavior of human neutrophils: power-low fluid. *Biophys. J.* 65:2078–2088.

2. Prosperetti, A., and G. Tryggvason, 2007. Computational Methods for Multiphase Flow. Cambridge University Press, Cambridge.

3. Yap, B., and R. D. Kamm, 2005. Mechanical deformation of neutrophils into narrow channels induces pseudopod projection and changes in biomechanical properties. *J. Appl. Physiol.* 98:1930–1939.

4. Yap, B., and R. D. Kamm, 2005. Cytoskeletal remodeling and cellular activation during deformation of neutrophils into narrow channels. *J. Appl. Physiol.* 99:2323–2330.

5. Zhelev, D. V., and R. M. Hochmuth, 1995. Mechanically stimulated cytoskeleton rearrangement and cortical contraction in human neutrophils. *Biophys. J.* 68:2004–2014.

6. Hochmuth, R. M., 2000. Micropipette aspiration of living cells. *J. Biomech.* 33:15–22.

7. Herant, M., V. Heinrich, and M. Dembo, 2005. Mechanics of neutrophil phagocytosis: behavior of the cortical tension. *J. Cell Sci.* 118:1789–1797.

8. Lu, L., Y. Feng, W. J. Hucker, S. J. Oswald, G. D. Longmore, and F. C. P. Yin, 2008. Actin stress fiber pre-extension in human aortic endothelial cells. *Cell Motil. Cytoskel.* 65:281–294.

9. Costa, K. D., W. J. Hucker, and F. C. P. Yin, 2002. Buckling of actin stress fibers: a new wrinkle in the cytoskeletal tapestry. *Cell Motil. Cytoskel.* 52:266–274.

10. Zhelev, D. V., D. Needham, and R. M. Hochmuth, 1994. A novel micropipet method for measuring the bending modulus of vesicle membranes. *Biophys. J.* 67:720–727.

11. Vanderlei, B., J. J. Feng, and L. Edelstein-Keshet, 2011. A computational model of cell polarization and motility coupling mechanics and biochemistry. *Multiscale Model. Simul.* 9:1420–1443.

12. Prass, M., K. Jacobson, A. Mogilner, and M. Radmacher, 2006. Direct measurement of the lamellipodial protrusive force in a migrating cell. *J. Cell Biol.* 174:767–772.

13. Cowan, A. E., L. Nakhimovsky, D. G. Myles, and D. E. Koppel, 1997. Barriers to diffusion of plasma membrane proteins form early during guinea pig spermiogenesi. *Biophys. J.* 73:507–516.

14. Postma, M., L. Bosgraaf, H. M. Loovers, and P. J. M. Van-Haastert, 2004. Chemotaxis: signaling modules join hands at front and tail. *EMBO Rep.* 5:35–40.

15. Holmes, W. R., B. Lin, A. Levchenko, and L. Edelstein-Keshet, 2012. Modelling cell polarization driven by synthetic spatially graded Rac activation. *PLoS Comput. Biol.* 8:e1002366.

16. Sako, Y., K. Hibino, T. Miyauchi, Y. Miyamoto, M. Ueda, and T. Yanagida, 2000. Single-molecule imaging of signaling molecules in living cells. *Single Mol.* 1:159–163.

17. Mori, Y., A. Jilkine, and L. Edelstein-Keshet, 2008. Wave-Pinning and cell polarity from a bistable reaction-diffusion system. *Biophys. J.* 94:3684–3697.

18. Mori, Y., A. Jilkine, and L. Edelstein-Keshet, 2011. Asymptotic and bifurcation analysis of wave-pinning in a reaction-diffusion model for cell polarization. *SIAM J. Appl. Math.* 71:1401–1427.